Structure enhancing filtering with the structure tensor

Rodrigo Morelatto* and Ricardo Biloti, IMECC/Unicamp & INCT-GP, Brazil

Abstract

The structure tensor is a very versatile tool used in general image processing. It can be used to detect edges, estimate coherency and local slopes. In this work we employ the structure tensor to estimate local slopes. We compare the slopes obtained by this tool with the slopes obtained by plane-wave destruction filters. Those two methods were tested against a synthetic and a real dataset. The slopes detected through the structure tensor were reliable and comparable to the ones obtained with plane-wave destruction filters. Finally, we present an application for the slopes detected by the structure tensor. We show how to employ them to filter seismic data along structures.

Introduction

Determining local slopes is of great interest in seismic data analysis. They can be used to accomplish many of time-domain imaging tasks, like normal moveout and prestack time migration (Ottolini, 1983; Fomel, 2007b). Local slopes can also be used to interpolate data and filter along seismic structures (Fomel, 2002; Liu et al., 2010). In this work we compare the local slopes obtained via the well established method of plane-wave destruction (Claerbout, 1992) to the ones obtained using the structure tensor (Bakker, 2002).

The structure tensor was applied to seismic data analysis and filtering many times before. Bakker (2002) gives a very comprehensive description of the applications of structure tensors to seismic data filtering. They can also be used to identify and create clusters of areas of interest in seismic data (Faraklioti and Petrou, 2005) and to edge preserving smoothing by diffusion filtering of seismic data (Hale, 2009; Lavialle et al., 2007).

Fehmers and Höcker (2003) have proposed to use the structure tensor to perform structure oriented filtering by anisotropic diffusion. This procedure results in structure simplification and make the seismic interpretation process more agile. Bakker (2002) also tried to address that problem by using orientation adaptive filtering and edge preserving filtering with the structure tensor. His work also features the use of the structure tensor to detect faults. In this paper we propose to study a third approach, by using structure prediction filtering (Liu et al., 2010). While Liu et al. (2010) advocate the use of plane-wave destruction to estimate dips, we propose to employ the dips detected by the tensor.

The structure tensor

The structure tensor is obtained by simple windowed smoothing operations and simple differentiation of the image. It is commonly used to detect lines and regions of interest in images.

The first order structure tensor is obtained by a first order Taylor approximation of the squared difference function. This function sums square differences of point-to-point image amplitudes between a fixed window W around the analysis point (x_0,t_0) and a window shifted by $\mathbf{x} \equiv (\Delta x, \Delta t)^T$. The squared difference function is defined as

$$E_{(x_0,t_0)}(\mathbf{x}) \equiv \sum_{(i,j)\in W} w_{i,j}\left[P(x_i+\Delta x, t_j+\Delta t) - P(x_i,t_j)\right]^2, \quad (1)$$

where W is a window around (x_0,t_0), $w_{i,j}$ are non-negative weights, and $P(x,t)$ is the image amplitude at the point (x,t). All the elements of the squared difference function are summarized in Figure 1.

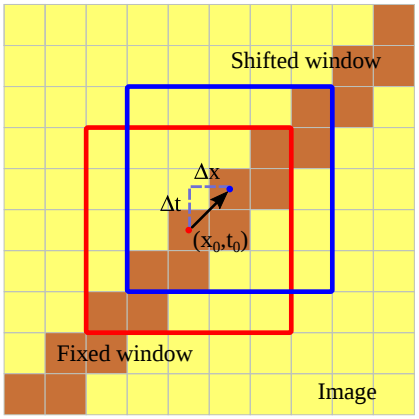

Figure 1: Parameters of the squared difference function. The red square indicates the fixed window around the point (x_0,t_0), and the blue one represents the window shifted by $(\Delta x, \Delta t)$. The arrow represents in this example the direction with no variations on the value of the squared difference function.

The first order Taylor approximation of P is

$$P(x_i+\Delta x, t_j+\Delta t) \approx P(x_i,t_j) + \Delta x P_x + \Delta t P_t, \quad (2)$$

where P_x and P_t are the data derivatives in x and t, respectively. Prior smoothing it is also necessary to estimate reliable derivative values from noisy raw data (Faraklioti and Petrou, 2005). By squaring both sides of the previous equation, we have a first order approximation to the squared difference

$$\begin{aligned}\left[P(x_i+\Delta x, t_j+\Delta t) - P(x_i,t_j)\right]^2 &\approx \left[\Delta x P_x + \Delta t P_t\right]^2 \\ &= \mathbf{x}^T \begin{bmatrix} P_x^2 & P_x P_t \\ P_x P_t & P_t^2 \end{bmatrix} \mathbf{x}. \end{aligned} \quad (3)$$

By substituting equation (3) on equation (1), we obtain the first order approximation for the squared difference function

$$\begin{aligned}\tilde{E}_{(x_0,t_0)}(\mathbf{x}) &\equiv \sum_{(i,j)\in W} w_{i,j}\,\mathbf{x}^T \begin{bmatrix} P_x^2 & P_xP_t \\ P_xP_t & P_t^2 \end{bmatrix}\mathbf{x} \\ &= \sum_{(i,j)\in W} \mathbf{x}^T \begin{bmatrix} w_{i,j}P_x^2 & w_{i,j}P_xP_t \\ w_{i,j}P_xP_t & w_{i,j}P_t^2 \end{bmatrix}\mathbf{x} \\ &= \mathbf{x}^T \begin{bmatrix} \langle P_x^2\rangle & \langle P_xP_t\rangle \\ \langle P_xP_t\rangle & \langle P_t^2\rangle \end{bmatrix}\mathbf{x} \\ &= \mathbf{x}^T\mathbf{M}\mathbf{x},\end{aligned} \tag{4}$$

The matrix $\mathbf{M}$ is known as the structure tensor and the symbol $\langle\cdot\rangle$ represents the average value produced by the smoothing procedure with weights $w_{i,j}$.

Eigenvalues and local image structure

The structure tensor is clearly symmetric. It is also positive semidefinite, i.e., $\mathbf{x}^T\mathbf{M}\mathbf{x} \geq 0$, for all $\mathbf{x}$. Indeed, from equations (3) and (4)

$$\mathbf{x}^T\mathbf{M}\mathbf{x} = \tilde{E}_{(x_0,t_0)}(\mathbf{x}) \geq 0, \tag{5}$$

as long as $w_{i,j}$ are nonnegative.

Since $\mathbf{M}$ is symmetric and positive semidefinite, all its eigenvalues are real and nonnegative and its eigenvectors are orthogonal. The structure tensor's eigenvalues and eigenvectors can be used to detect lines, borders and regions with constant image intensity.

When there is a linear feature in the image, as sketched in Figure 1, only one possible direction admits no variations of the squared difference function value. This direction is parallel to the linear feature. Recalling equation (4), and assuming $0 = E(\mathbf{x}) \approx \tilde{E}(\mathbf{x})$, for $\mathbf{x}$ in the direction parallel to the linear feature observed in the image we have

$$\mathbf{x}^T\mathbf{M}\mathbf{x} \approx 0. \tag{6}$$

In fact, by means of spectral decomposition of $\mathbf{M}$, it is possible to show that such direction is an approximated eigenvector of $\mathbf{M}$, associated with an eigenvalue close to zero. The other eigenvalue is greater than zero, because it corresponds to the eigenvector orthogonal to the linear feature.

Both eigenvalues λ_1 and λ_2, solution of the characteristic equation of $\mathbf{M}$, are explicitly given by

$$\lambda_1 = \frac{1}{2}\left[\left\langle P_x^2\right\rangle + \left\langle P_t^2\right\rangle + \sqrt{\left(\left\langle P_x^2\right\rangle + \left\langle P_t^2\right\rangle\right)^2 - 4\left(\left\langle P_x^2\right\rangle\left\langle P_t^2\right\rangle - \langle P_xP_t\rangle^2\right)}\right] \tag{7}$$

and

$$\lambda_2 = \frac{\langle P_x\rangle\langle P_t\rangle - \langle P_xP_t\rangle^2}{\lambda_1}. \tag{8}$$

By definition $\lambda_1 \geq \lambda_2$ and both are nonnegative. Besides, any eigenvector associated with λ_2 will be parallel to the direction of a detected linear feature in the image. It is straightforward to determine $v_2 = \alpha(\langle P_xP_t\rangle, \lambda_2 - \langle P_x^2\rangle)^T$, for any nonzero scalar α, and v_1 orthogonal to v_2. Therefore, we can estimate the local slope using the orientation of either v_1 or v_2, as

$$\sigma = \begin{cases} \dfrac{\lambda_2 - \langle P_x^2\rangle}{\langle P_xP_t\rangle}, & \text{if } \langle P_xP_t\rangle \gg 0 \\ -\dfrac{\langle P_xP_t\rangle}{\lambda_1 - \langle P_x^2\rangle}, & \text{otherwise.} \end{cases} \tag{9}$$

Comparison of slope estimations

We propose to study the tensor properties using the synthetic sedimentary data of Figure 2 and the historic field dataset from Figure 3. Proposed by Claerbout (1992), the first dataset is composed by 200×200 pixels, spaced by 8 m in the x axis and 4 ms in the t axis. The second dataset is a time-migrated seismic image from a historic Gulf of Mexico dataset (Claerbout and Green, 2010). It is composed by 250×876 pixels with the time sampling of 4 ms, and spacing between traces considered as unitary. The data was also filtered with an AGC filter using triangular weights and half-second window.

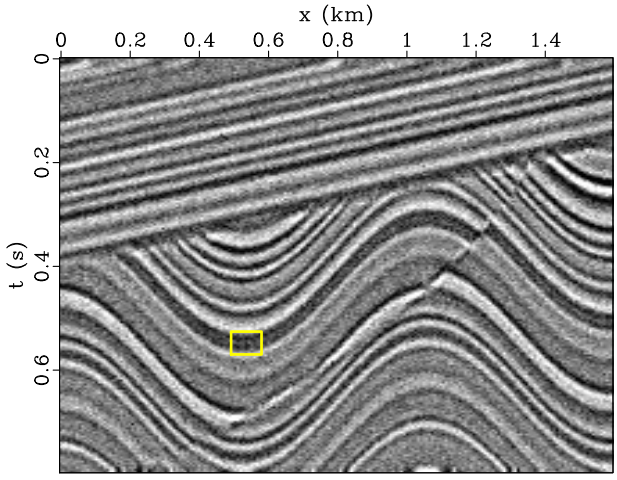

Figure 2: Synthetic sedimentary model and the window size used for the structure tensor.

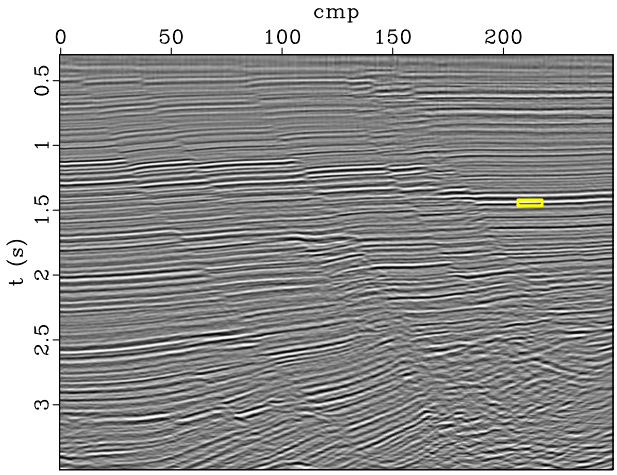

Figure 3: Real historic dataset from the Gulf of Mexico and the window size used for the structure tensor.

In our computational tests, the W window size in the structure tensor formula was 11×11 samples. This size should reflect the characteristic size of the texture of interest (Weickert, 1999), as show in figures 2 and 3. The window samples were weighted by

$$w_{i,j} = \frac{1}{\varsigma^2 \pi} \exp\left(-\frac{i^2 + j^2}{\varsigma^2}\right), \tag{10}$$

with $\varsigma = 3.5$. Those weights were also used in the Gaussian smoothing process for the data derivatives estimation, but with $\varsigma = 2.5$, to avoid over smoothing.

To judge the quality of the slopes obtained by the structure tensor we compare its results with the ones obtained by other well established methods. We choose to compare it with the well-known method of plane-wave destruction (Claerbout, 1992), as formulated by Fomel (2002). It treats the plane-wave filter as a time-distance (t-x) prediction-error filter. We employed the version implemented in the Madagascar package (Madagascar Development Team, 2012).

By comparing the figures 4 and 5, for the synthetic data, we can observe that both methods achieved similar results. This is also observed for the real data, by comparing figures 6 and 7. Nevertheless, the structure tensor has the advantage of being faster to run and simpler to implement.

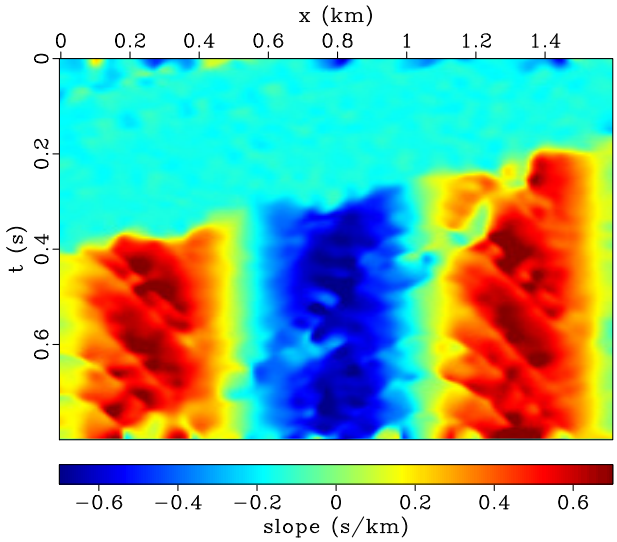

Figure 4: Local slopes estimated with the structure tensor for the synthetic data.

Structure prediction filtering

There are many ways to accomplish structure-enhancing filtering of a seismic image, like diffusion filtering of seismic data (Lavialle et al., 2007) or steering Gaussian elongated windows along local slope patterns (Haglund, 1991). For performance testing purposes, we choose to filter along the structures using plane-wave prediction (Liu et al., 2010). The filtering scheme is shown in Figure 8.

A trace can be predicted by shifting its neighbours according to the local seismic event slopes. Consider the prediction operator $\mathbf{P}_{i,j}(\sigma_i)$ as an operator for prediction of trace j from trace i, according to the local slope pattern σ_i (see

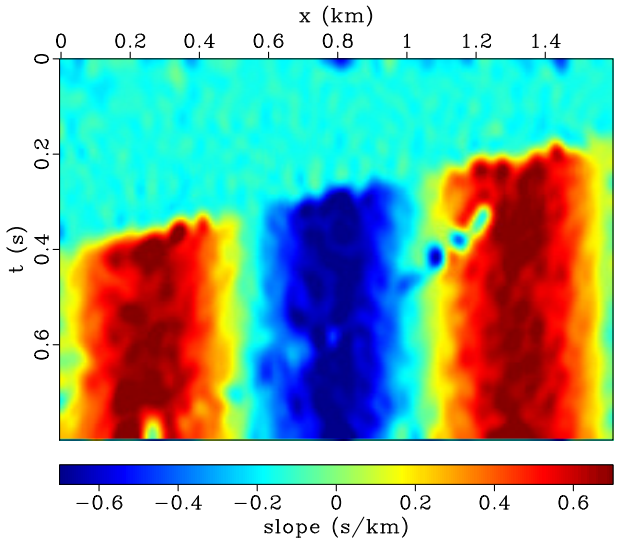

Figure 5: Local slopes estimated with the plane-wave destructor for the synthetic data.

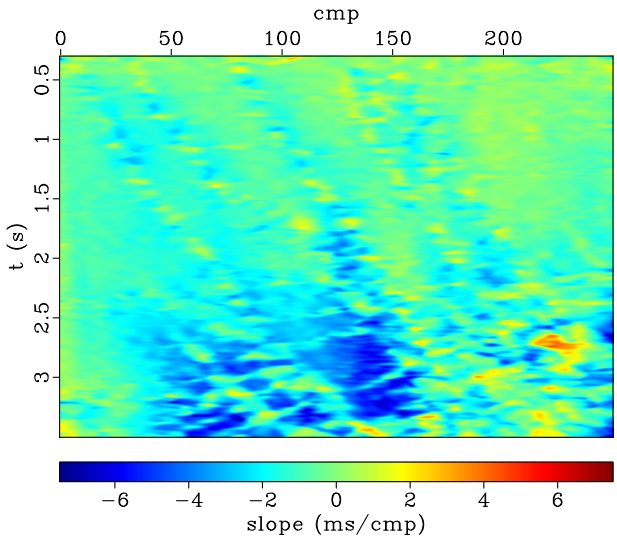

Figure 6: Local slopes estimated with the structure tensor for the real data.

e.g. Fomel (2002) and Fomel (2010) for further details). It's possible to predict a trace from a distant neighbor by simple recursion. So, predicting trace k from trace 1 is simply

$$\mathbf{P}_{1,k} = \mathbf{P}_{k-1,k} \cdots \mathbf{P}_{2,3} \mathbf{P}_{1,2}. \tag{11}$$

In this work we propose the use of the structure prediction with the dips estimated by the structure tensor, instead of using the ones estimated with plane-wave destruction. After estimating the slopes, we predict a trace from its neighbors and stack the predicted traces with the original one. In that way we accomplish the structure filtering, as shown in figures 9 and 11, for the real and synthetic datasets.

In Figure 9 the blurring of data near the fault and the interface between the folded and plane regions is clear. This is further confirmed by the difference section, in Figure 10.

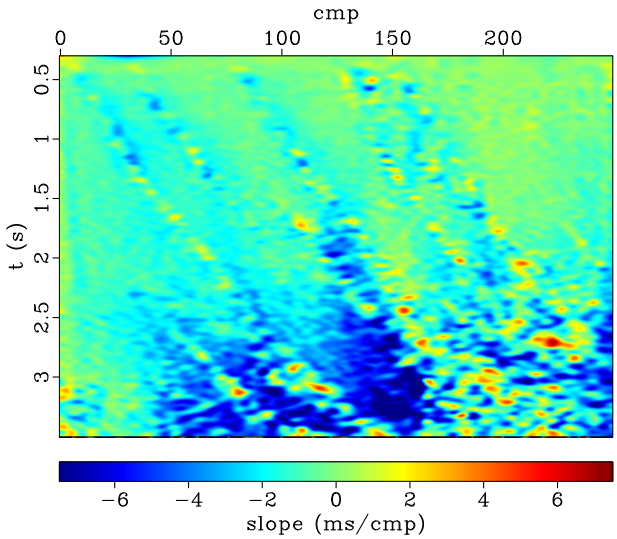

Figure 7: Local slopes estimated with the plane-wave destructor for the real data.

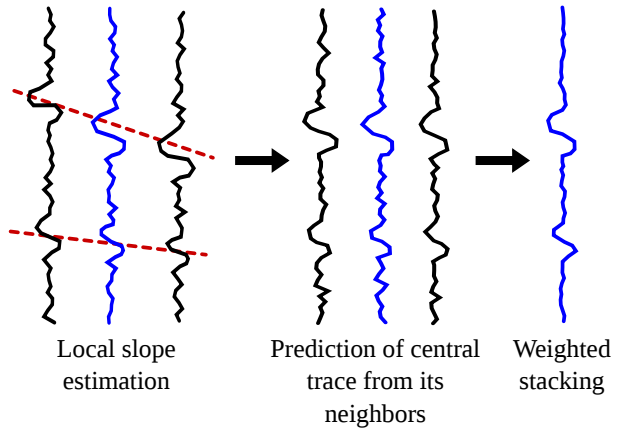

Figure 8: Prediction filtering scheme for the trace in blue.

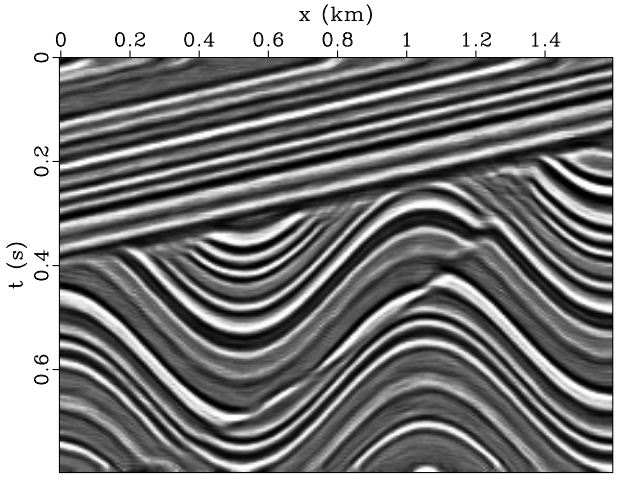

Figure 9: Structure prediction filtering for the synthetic data.

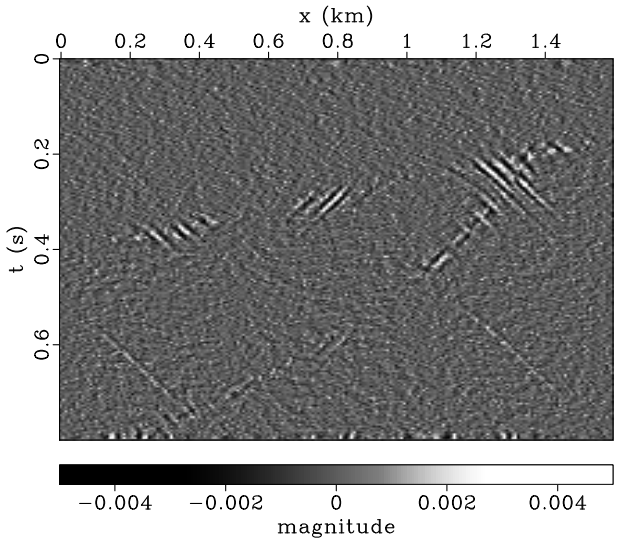

Figure 10: Difference between filtered and original synthetic data.

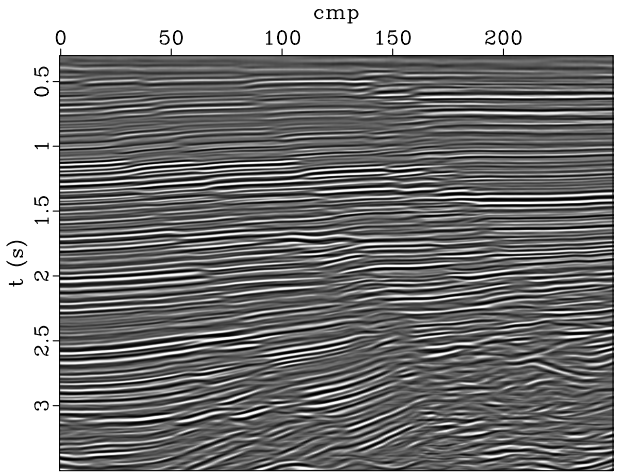

Figure 11: Structure prediction filtering for the real data.

This blurring effect is also visible on the real data, as shown in Figure 11, and in the difference section, in Figure 12. Another problem occurs in areas without well defined local slopes. In these areas the filtering process creates false seismic structures, as illustrated in the lower right corner of Figure 11.

To prevent these effects, we decided to follow Liu et al. (2010) approach and improve the structure filtering by using similarity based weights for the stacking step. Those weights are computed with the local similarity proposed by Fomel (2007a). In this formulation the similarity varies smoothly, being close to one when the two traces compared are locally similar and approaching zero when they differ.

To further improve the data staking we also employed a Gaussian taper. This produces lower weights in stacking for traces predicted from traces far from the original one, which diminishes some prediction errors in the stacking (Liu et al.,

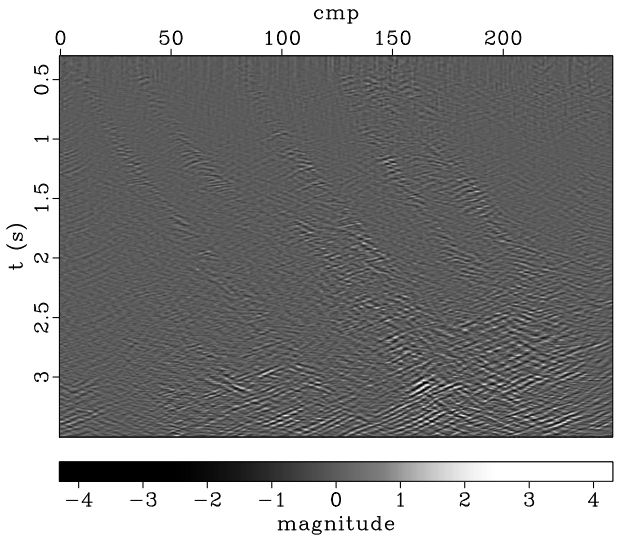

Figure 12: Difference between filtered and original real data.

2010). We multiply each trace by

$$w_k = \exp\left(-\frac{k^2}{\zeta^2}\right), \tag{12}$$

where w_k is a Gaussian weight function, k is the index offset between the original and the predicted traces, i.e. for the original trace $k = 0$, for a trace predicted using an immediate neighbour $k = 1$. The ζ parameter just alters the shape of the Gaussian. For the synthetic data, we used $\zeta = 0.02$ and for the real data, $\zeta = 2$.

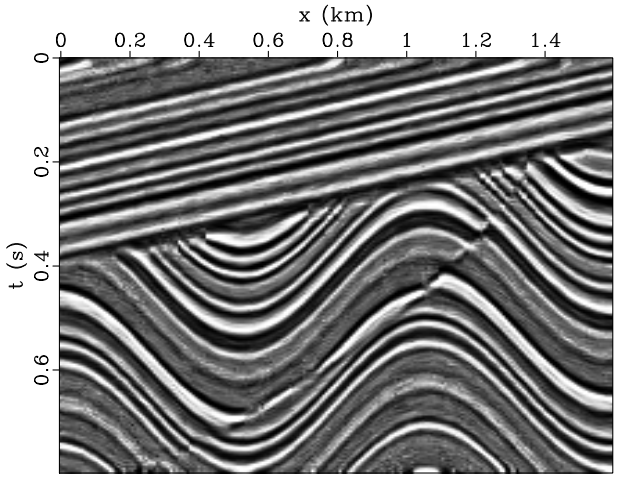

Figure 13: Structure prediction filtering with similarity for the synthetic data.

Finally, the filtering results using the six nearest neighbour traces for the prediction step with similarity stacking weights is shown in Figure 13, for the synthetic data. The results for the real data are illustrated in Figure 15. We can see that the noise was attenuated and the seismic events were preserved. Also there are very little smearing of the faults and other interfaces, as shown in the difference between

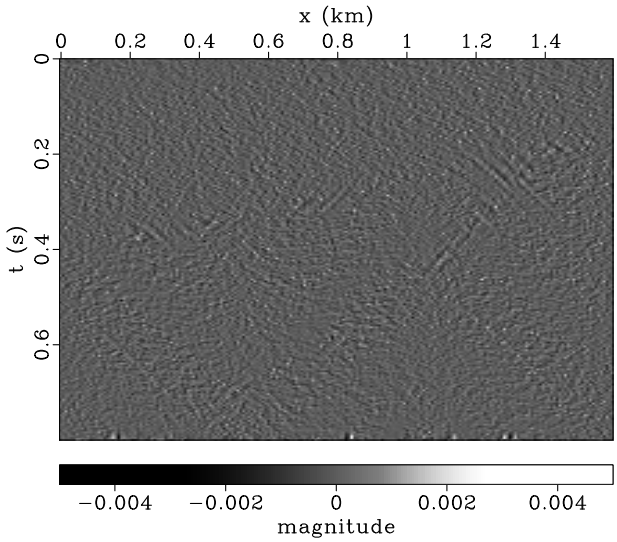

Figure 14: Difference between the similarity enhanced filtered data and original synthetic data.

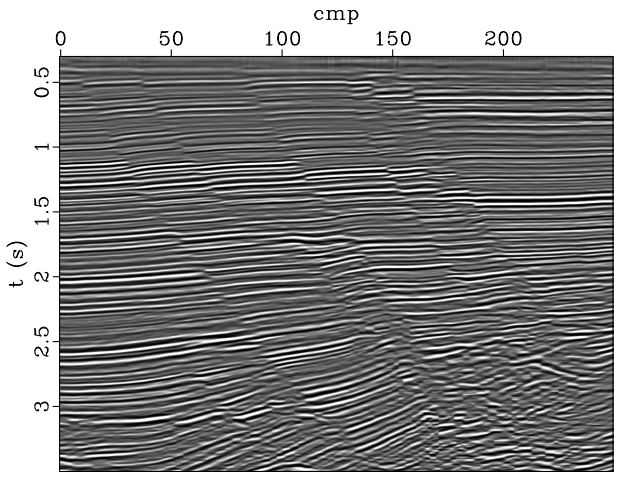

Figure 15: Structure prediction filtering with similarity for the real data.

the original data and the filtered data in figures 14 and 16, for the synthetic and real data, respectively.

That is also evident by comparing this last figure with the original filtering differences, depicted in Figure 10, for the synthetic data. Thanks to the local similarity, no false events were created in this filtering, as depicted comparing figures 11 and 15.

Conclusions

The structure tensor is highly correlated with the image local structure. It provides a fairly good and robust estimation for seismic data local slopes. The values obtained for the slopes are also very close to the ones obtained by the plane-wave destruction method tested. These two statements are also confirmed by Morelatto (2013), using other synthetic datasets to perform further tests. One point to keep in mind is that care should be taken on the smoothing prior to the data differentiation, to not blur features of interest,

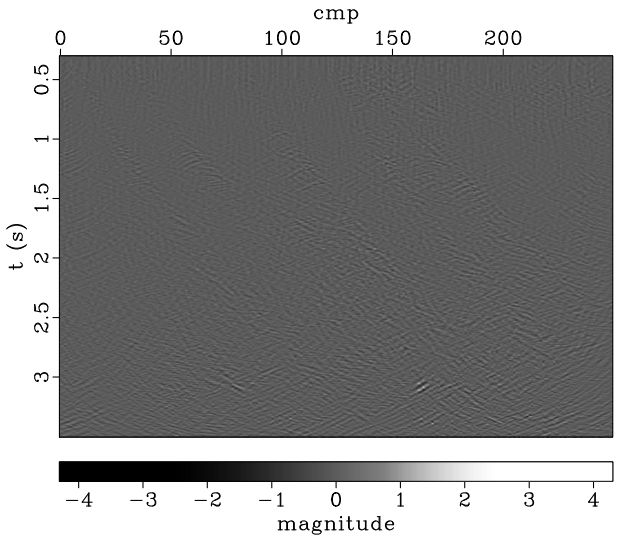

Figure 16: Difference between the similarity enhanced filtered data and original real data.

like reflector terminations. Also, one should be careful on choosing the window size. It should reflect the characteristic size of the features of interest (Weickert, 1999).

For performance testing purposes, we used the structure tensor slopes for structure oriented filtering. As seen in figures 13 and 15, the results were very satisfactory, removing mostly noise from the data. These results assert the quality of the structure-tensor based slopes. One of the advantages of this method is the easy implementation and fast runtime, since it is basically composed of weighted local sums over data. In the near future we intend to further test the structure tensor filtering capabilities. Working interactively, it is also possible to deal with conflicting dips.

References

Bakker, P., 2002, Image structure analysis for seismic interpretation: PhD thesis, Delft University of Technology, Delft, Netherlands.

Claerbout, J., 1992, Earth soundings analysis: Processing versus inversion: Blackwell Scientific Publications, **6**.

Claerbout, J., and I. Green, 2010, Basic earth imaging: Stanford University.

Faraklioti, M., and M. Petrou, 2005, The use of structure tensors in the analysis of seismic data, *in* Mathematical Methods and Modelling in Hydrocarbon Exploration and Production: Springer, volume **7** *of* Mathematics in Industry, 47–88.

Fehmers, G., and C. Höcker, 2003, Fast structural interpretation with structure-oriented filtering: Geophysics, **68**, 1286–1293.

Fomel, S., 2002, Applications of plane-wave destruction filters: Geophysics, **67**, 1946–1960.

———, 2007a, Local seismic attributes: Geophysics, **72**, A29–A33.

———, 2007b, Velocity-independent time-domain seismic imaging using local event slopes: Geophysics, **72**, S139–S147.

———, 2010, Predictive painting of 3D seismic volumes: Geophysics, **75**, A25–A30.

Haglund, L., 1991, Adaptive multidimensional filtering: PhD thesis, Linköping University, Linköping, Sweden.

Hale, D., 2009, Structure-oriented smoothing and semblance: CWP Report 635, Center Wave Phenomena.

Lavialle, O., S. Pop, C. Germain, M. Donias, S. Guillon, N. Keskes, and Y. Berthoumieu, 2007, Seismic fault preserving diffusion: Journal of Applied Geophysics, **61**, 132–141.

Liu, Y., S. Fomel, and G. Liu, 2010, Nonlinear structure-enhancing filtering using plane-wave prediction: Geophysical Prospecting, **58**, 415–427.

Madagascar Development Team, 2012, Madagascar software, version 1.4. http://www.ahay.org/.

Morelatto, R., 2013, Seismic data filtering with the structure tensor: Master's thesis, University of Campinas, Campinas, Brazil.

Ottolini, R., 1983, Velocity independent seismic imaging: SEP-37: Stanford Exploration Project, 59–68.

Weickert, J., 1999, Coherence-enhancing diffusion filtering: International Journal of Computer Vision, **31**, 111–127.

Acknowledgments

This work was supported by the National Institute of Petroleum Geophysics (INCT-GP/CNPq), Brazil, and by the sponsors of the WIT Consortium.